

## A NEW METHOD FOR DETERMINATION OF THE THEORETICAL REDUCTION AMOUNT FOR WIDE-THICK SLAB DURING THE MECHANICAL REDUCTION PROCESS

C.-H. Wu \*, J.-H. Zeng, G.-R. Wu, X. Xie, M. Zhang

Pangang Group Research Institute Co., Ltd., Panzhihua, Sichuan, China

(Received 22 June 2020; Accepted 05 January 2021)

### Abstract

Mechanical soft reduction (MSR) is an effective method for elimination of the centerline segregation and porosity of the continuous casting steel slab, and the reduction amount is a key parameter that determines whether the MSR could be applied successfully. In the present work, a 2D heat transfer model was developed for predicting the non-uniform solidification of the wide-thick slab. The measured shell thickness by nail shooting experiment and the measured slab surface temperature by infrared camera were applied to validate the 2D heat transfer model. A new calculation method of theoretical reduction amount that could consider the influence of non-uniform solidification of the wide-thick slab was then derived. Based on the predicted temperature field by the 2D heat transfer model and the newly-proposed calculation method, the required theoretical reduction amount and reduction gradient/rate for the wide-thick slab were calculated and discussed. The difference between the newly-proposed method and the previous method, the influence of the casting speed and slab thickness on the required theoretical reduction amount and reduction gradient/rate were also investigated.

**Keywords:** Theoretical reduction amount; Mechanical soft reduction; Continuous casting; Wide-thick slab; Non-uniform solidification

### 1. Introduction

Centerline segregation and porosity are common internal defects in continuous casting steel, which brings a number of adverse effects [1, 2]. For example, the severe centerline segregation and porosity can lead to delamination of the rolled plate, center burst, wire breakage in the subsequent processing and obviously deteriorate the impact properties and weldability of the final products. To alleviate these two defects, electromagnetic stirring, thermal soft reduction, mechanical soft reduction (MSR) and casting with low superheat, etc. were proposed and applied [3, 4]. During these counter measures, MSR has been proved to be the best way to minimize the centerline segregation and porosity due to its flexibility and efficiency [5, 6].

The principle of MSR is to implement a mechanical reduction amount before the strand solidification end to compensate the solidification shrinkage in the mushy region and interrupt the suction flow of the interdendritic solute-enriched residual melt toward the strand center [7, 8], and reduction zone and

reduction amount are the two critical process parameters that determine the successful application of MSR. Reduction amount, as one of the critical process parameters, represents the strand thickness reduction during the implementation of MSR, which had been investigated by the previous researchers with plant trials [4, 9, 10] or mathematical models [11-21]. When the practical reduction amount is determined by adopting mathematical models, two critical issues should be firstly resolved: the theoretical reduction amount and the reduction efficiency. The theoretical reduction amount [20, 21] represents the required minimum reduction amount that could just compensate the solidification shrinkage in the strand mushy region without considering the consumption of the reduction amount due to the deformation of the solidified shell. During the implementation of MSR, elongation deformation and broadening deformation of the casting strand simultaneously occurs, which hinders the transfer of reduction amount from the strand surface to its internal mushy region. To estimate the efficiency of the reduction amount that could effectively transfer through the solidified shell to the

---

Corresponding author: [wch\\_neu@126.com](mailto:wch_neu@126.com)

<https://doi.org/10.2298/JMMB200622010W>



mushy region, reduction efficiency [13-17] was proposed and studied. Based on the theoretical reduction amount and reduction efficiency, the required practical reduction amount [18-21] for MSR could be determined.

With respect to the study on theoretical reduction amount, Lin et al. [11, 12] established a mathematical model of theoretical reduction amount for the slab continuous casting with the assumption of invariant total mass flow in any transverse section of the casting strand during the implementation of MSR. With this model, Lin et al. investigated the influence of casting speed [11] and steel grade [12] on the theoretical reduction rate and reduction gradient that respectively denoted the required theoretical reduction amount per unit time and per unit strand length. Ji et al. [18, 21] deduced the required compensated area in the strand liquid core according to mass flow difference between two MSR points during the determination of the practical reduction amount for bloom continuous casting. Liu et al. [19, 20] quantitatively calculated the volume shrinkage in the strand center interdendritic region through the evaluation of the changing melt density before the practical reduction amount was determined for bloom [19] and slab [20] continuous casting. By considering the effect of height reduction at each pinch roller and the solidification shrinkage, Rogberg et al. [22] developed an analytical mathematical model and quantitatively investigated the fluid flow, porosity center segregation in CC high carbon and stainless steel blooms under condition of different reduction amount. The required compensated area [18, 21] and volume shrinkage [19, 20] mentioned above essentially also reflected the needed theoretical reduction amount that could just compensate the solidification shrinkage of the strand mushy region without considering the consumption of reduction amount due to the elongation deformation and the broadening deformation of the solidified shell.

The solidification process of the casting strand directly determines the characteristics of the solidification shrinkage in its mushy region and thus significantly influences the required theoretical reduction amount. Compared with the continuous casting steel with a small section size, the solidification of the wide-thick slab shows obvious non-uniformity along its width direction due to the non-uniform cooling water flux distribution in the secondary cooling region [8, 23] of the continuous caster. In the previous studies [11, 12, 18-21], the

mushy region was usually taken as a whole to calculate the theoretical reduction amount. However, these methods are proved to be no longer suitable for the wide-thick slab because the influence of the solidification non-uniformity of the wide-thick slab could not be well taken into consideration. Plant results, as indicated in Figure 1, show that the centerline segregation and porosity of the wide-thick slab, especially the region within the rectangular boxes, could not be effectively alleviated by the MSR if the practical reduction amount was determined based on the calculated theoretical reduction with the previous methods.

In order to overcome the drawbacks of the previous methods, a new calculation method of the theoretical reduction amount that could well consider the solidification non-uniformity of the wide-thick slab was developed in the present paper. The non-uniform solidification of the wide-thick slab was calculated with a 2D heat transfer model. Based on the predicted results by the 2D heat transfer model, mushy region of the wide-thick slab was assumed to consist of micro-units, and the required theoretical reduction amounts for different positions of the wide-thick slab along its width direction were derived by evaluating the total volume shrinkage of the micro-units at the corresponding position. With this newly-proposed method, the theoretical reduction amount, reduction rate, and reduction gradient under different casting speeds were investigated.

## 2. Heat Transfer Model

### 2.1. Model Description

Heat transfer of the wide-thick slab directly determines the solidification shrinkage in its mushy region and thus is the prerequisite to derive the theoretical reduction amount. Based on some simplified assumptions [24], a 2D heat transfer model of one quarter of the slab transverse section, as shown in Figure 2, was established for predicting the non-uniform solidification of the wide-thick slab. 4-nodes quadrilateral elements with 5mm sides were used to mesh the calculation domain. During the calculation, automatic time step was employed, and the maximum and minimum time step were respectively 0.01s and 1s. The research steel grade was a peritectic steel, and its main chemical composition is shown in Table 1. Detailed parameters about the structure and the cooling region divisions of the wide-thick slab continuous caster can be found in the previous work [23].

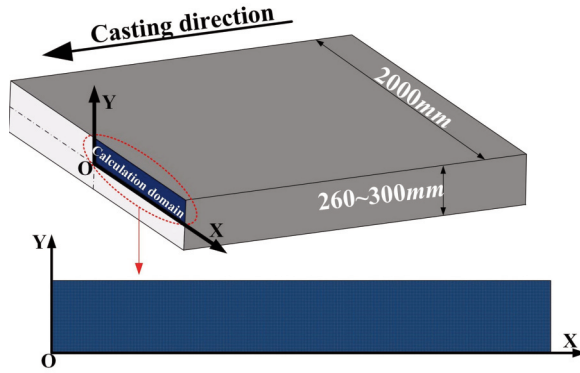


Figure 1. Macrograph of the transverse section of 2000mm×280mm section wide-thick slab



**Table 1.** Main chemical composition of the research steel in weight%.

C	Si	Mn	P	S
0.17	0.15	0.60	0.015	0.01



**Figure 2.** Schematic of the 2-D heat transfer model

The heat transfer behavior of the mathematical model can be described by the two-dimensional transient heat conduction equation:

$$\frac{\partial}{\partial x} \left( \lambda \frac{\partial T}{\partial x} \right) + \frac{\partial}{\partial y} \left( \lambda \frac{\partial T}{\partial y} \right) + \rho L \frac{\partial f_s}{\partial t} = \rho c \frac{\partial T}{\partial t} \quad (1)$$

where  $T$  and  $t$  are respectively the temperature in  $^{\circ}\text{C}$  and calculation time in  $\text{s}$ ;  $\rho$ ,  $c$ , and  $\lambda$  are the temperature-dependent density, specific heat, and conductivity in  $\text{kg}/\text{m}^3$ ,  $\text{J}/(\text{kg}\cdot^{\circ}\text{C})$ , and  $\text{W}/(\text{m}\cdot^{\circ}\text{C})$ , respectively;  $L$  is the latent heat of steel solidification equal to  $272000 \text{ J}/\text{Kg}$ .

The calculation time  $t$  is related to the casting speed and the distance of the 2D heat transfer model from the meniscus:

$$t = \frac{Z}{V_{cast}} \quad (2)$$

where  $Z$  is the distance of the 2D heat transfer model from the meniscus,  $\text{m}$ ;  $V_{cast}$  is the casting speed,  $\text{m}\cdot\text{s}^{-1}$ . In order to acquire more accurate thermal material properties of the peritectic steel, the phase fraction evolution of the peritectic steel, as shown in Figure 3(a), was calculated with a micro-segregation model that had been described in detail in the previous work [8].  $f_{\delta}$ ,  $f_{\gamma}$ ,  $f_s$ , and  $f_L$  in Figure 3(a) are the fraction of  $\delta$ -Fe,  $\gamma$ -Fe, solid and liquid, respectively, and  $f_s$  is equal to the sum of  $f_{\delta}$  and  $f_{\gamma}$ . Based on the derived phased fraction evolution, thermal material properties of density, conductivity and enthalpy, as shown in Figure 3(b) ~ (d), were then calculated with weighted averaging of the phase fraction method [25]. It should be noted that the thermal conductivity of the liquid

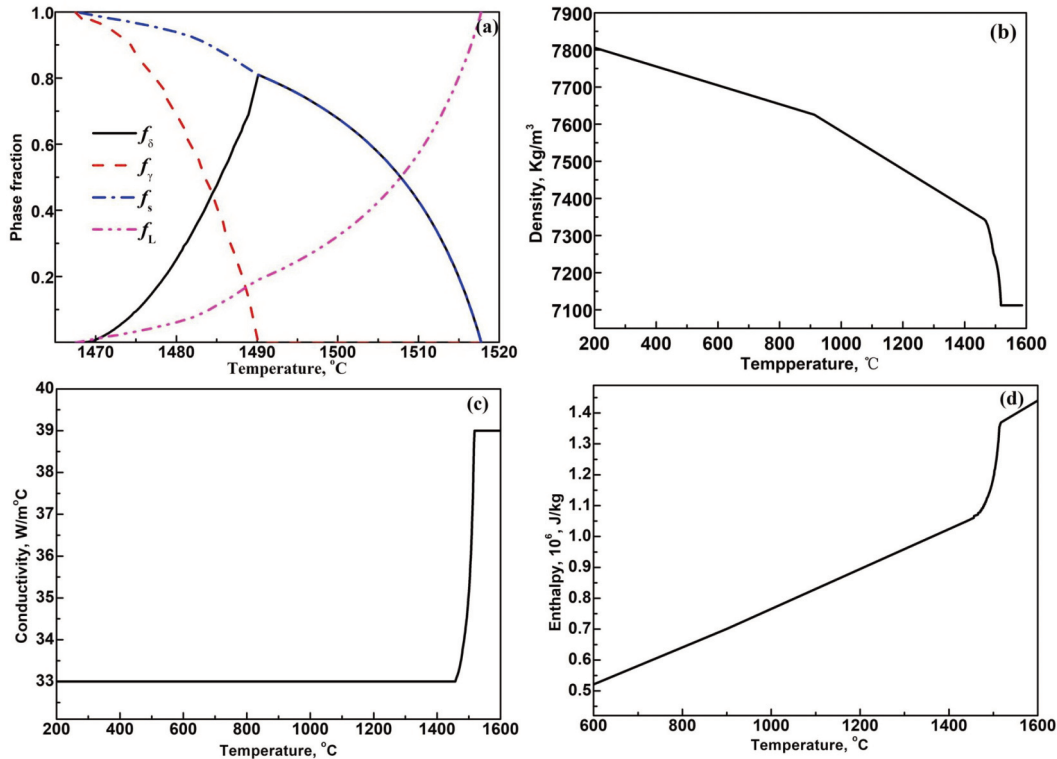


**Figure 3.** Evolution of the (a) phase fraction, (b) conductivity, (c) density and (d) enthalpy with temperature



steel was a few times higher compared to that of the solid state for considering the enhanced effect of molten steel flow on the heat conduction of steel [8, 10, 26].

Cooling boundary conditions, such as heat flux in mold ( $q_{mold}$ ), heat transfer coefficient between the casting strand and cooling water ( $h_w^i$ ), heat transfer coefficient of radiation ( $h_{rad}$ ) below the mold could be calculated with the following equations [8, 23], respectively:

$$q_{mold} = 2.688 - B\sqrt{t} \quad (3)$$

$$h_{spray}^i = -\alpha_i W_i^{0.55} (1 - 0.075T_w) \quad (4)$$

$$h_{rad} = \varepsilon \cdot \sigma \cdot (T_{surf}^2 + T_{env}^2) (T_{surf} + T_{env}) \quad (5)$$

where  $B$  is a coefficient depending on the mold cooling condition;  $t$  is the casting time in mold, s;  $\alpha_i$  is the modified parameter of  $i^{\text{th}}$  cooling zone;  $W_i$

represents the cooling water flux density along the slab width direction,  $L/(m^2 \cdot \text{min})$ ;  $T_w$  is the cooling water temperature, °C.  $\varepsilon$  is the emissivity, 0.8;  $\sigma$  is the Stefan–Boltzmann coefficient,  $5.67 \times 10^{-8} (W/m^2 K^4)$ ;  $T_{surf}$  and  $T_{env}$  respectively denote the temperature of strand surface and the environment, K.

It should be noted that the cooling water flux distribution ( $W_i$ ) was measured to calculate  $h_w^i$  in Eq.(4). Figures 4(a) and (b) respectively show the nozzle arrangement and the measured cooling water flux distribution in secondary cooling zone 5 ~ 8. The water flux percentage at different positions along the slab width direction in Figure 4(b) was calculated with the real measured water flux at the corresponding position divided by the measured water flux at the slab center. It can be seen from Figure 4(b) that the water flux distribution percentage under different water and air pressures was similar and continuously decreased from slab center to corner.

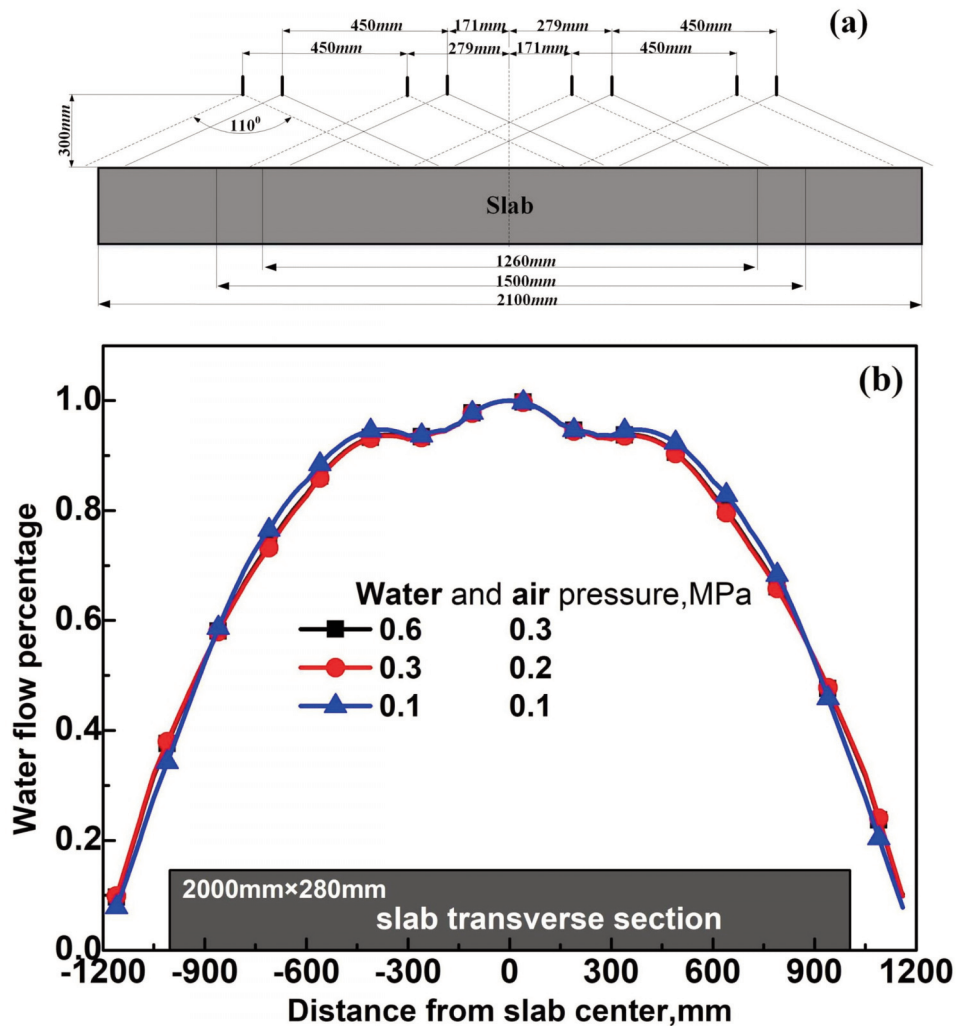


Figure 4. (a) Nozzle arrangement and (b) the corresponding measured water flux distribution along slab width in zone 5-8

## 2.2. Model Validation

To verify the heat transfer model, slab surface temperature and shell thickness at the slab 1/2 and 1/8 width were respectively measured by infrared camera (A40, FLIR) and nail shooting method (nail shooting device is shown in Figure 5) at the strand position of 20.49 m and 22.13 m when the 2000 mm × 280 mm section size slab was cast at 0.8 m·min<sup>-1</sup>. Figures 6(a) and (b) compare the predicted temperature and shell thickness with the measured results. It can be seen that both the predicted slab surface temperature and the shell thickness agree well with the measured results, and the absolute value of the relative error between predicted and measured results were less than 2.3% for slab surface temperature and less than 2.5% for shell thickness. Furthermore, due to the continuously decreasing cooling water flux distribution from slab center to its corner (as shown in Figure 4), the surface temperature and shell thickness at 1/2 width significantly differed from that at 1/8 width, and the slab surface temperature and shell thickness at 1/8 width were respectively higher and thinner than that at 1/2 width.

## 3. Calculation Method of Theoretical Reduction Amount

For fully considering the solidification non-uniformity of the wide-thick slab during the determination of the theoretical reduction amount, the slab mushy region was assumed to consist of rows of micro-units along the slab width direction, and Figure 7 schematically shows the micro-units in one row at the mid-width of the wide-thick slab.

At the beginning time of MSR, mass of each micro-unit can be calculated as:

$$m_i^0 = v_i^0 \cdot \rho_i^0 \quad (6)$$

where  $m_i^0$ ,  $v_i^0$ , and  $\rho_i^0$  respectively represent the mass, volume, and density of micro-unit  $i$ , and the superscript and the subscript respectively denote the reduction time and the number of micro-unit.

During the implementation of MSR, mass of each micro-unit at reduction time  $t$  can be calculated as:

$$m_i^t = v_i^t \cdot \rho_i^t \quad (7)$$

If the solidification shrinkage of each micro-unit

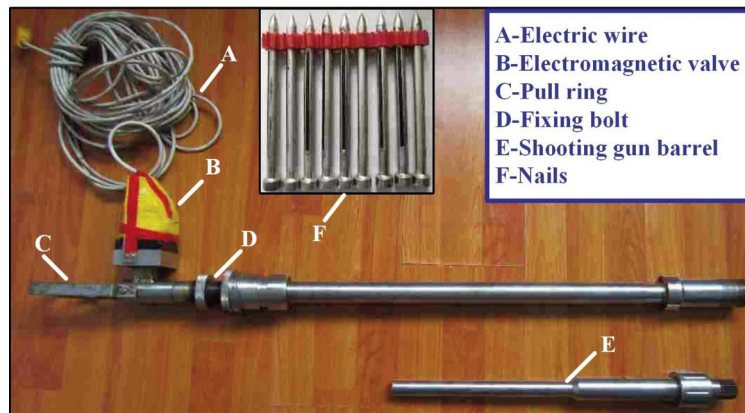


Figure 5. Nail shooting device

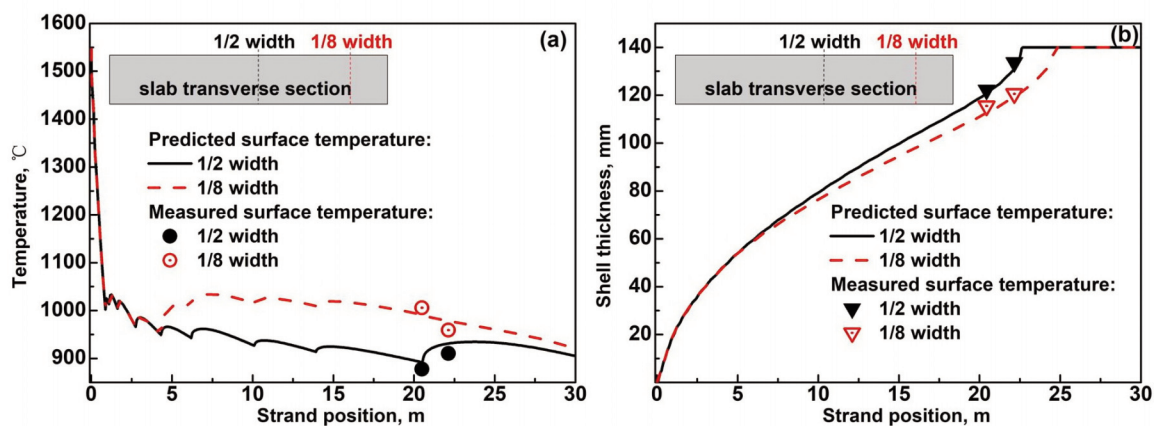


Figure 6. Comparison between the predicted and the measured (a) slab surface temperature and (b) shell thickness

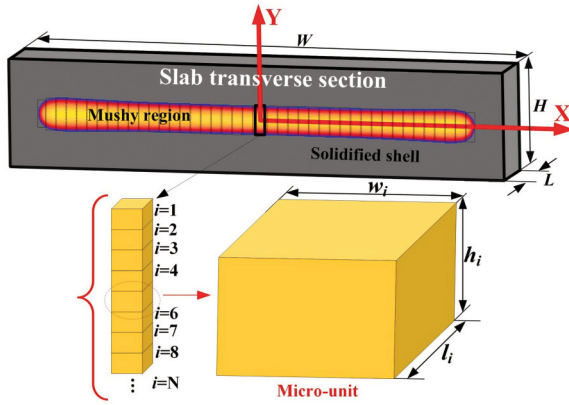


Figure 7. Schematic of the micro-units in one row in the mushy region of the wide-thick slab

in the mushy region can be just compensated by MSR, the suction flow of the interdendritic solute-enriched liquid steel can be prevented. As a result, the mass of each micro-unit remained constant during the implementation of MSR, which can be expressed by the following equation:

$$m_i^0 = m_i^t \quad (8)$$

Combining Eqs. (3) ~ (5), the volume shrinkage of each micro-unit can be calculated as:

$$\Delta v_i^t = v_i^0 - v_i^t = v_i^0 \left( 1 - \frac{\rho_i^0}{\rho_i^t} \right) \quad (9)$$

where  $\Delta v_i^t$  denotes the volume shrinkage of micro-unit  $i$  at the reduction time  $t$ .

The required reduction amount for compensating the volume shrinkage of micro-unit  $i$  can be derived as:

$$\Delta h_i^t = \frac{\Delta v_i^t}{l_i w_i} = \frac{v_i^0 \left( 1 - \frac{\rho_i^0}{\rho_i^t} \right)}{l_i w_i} \quad (10)$$

where  $\Delta h_i^t$ ,  $l_i$  and  $w_i$  respectively represent the required reduction amount, length and width of micro-unit  $i$ .

Theoretical reduction amount represents the minimum reduction amount that could just compensate the volume shrinkage in the slab mushy region without considering the consumption of reduction amount due to the elongation deformation and broadening deformation of the solidified shell. This means that the length  $l_i$  and the width  $w_i$  of micro-unit  $i$  can be considered to remain invariable during the determination of the theoretical reduction amount. Therefore, Eq. (7) can be further simplified as:

$$\Delta h_i^t = h_i \left( 1 - \frac{\rho_i^0}{\rho_i^t} \right) \quad (11)$$

where  $h_i$  is the thickness of micro-unit  $i$ .

The required theoretical reduction amount at any position of the wide-thick slab along its width direction can be determined by adding up the required theoretical reduction amount of all the micro-units in the row at the corresponding position:

$$\Delta H^t = \sum_{i=1}^N \Delta h_i^t = \sum_{i=1}^N h_i \left( 1 - \frac{\rho_i^0}{\rho_i^t} \right) \quad (12)$$

where  $\Delta H^t$  represents the required theoretical reduction amount at one position of the wide-thick slab at the reduction time  $t$ ;  $N$  is the total number of the micro-units in a row at one position along the slab width direction.

The calculation model of the theoretical reduction amount was solved with the help of the established heat transfer model in Section 2.1. The elements in the heat transfer model were regarded as the micro-units in the calculation model of the theoretical reduction. This means the value of  $N$  was equal to the number of elements of the 2D heat transfer model at one position along the slab thickness direction. During the solving process, the thickness of each element in the heat transfer model (corresponding to  $h_i$  in Eq.(9)) was specified, and the density of each element (corresponding to  $\rho_i^0$  and  $\rho_i^t$  in Eq.(9)) could be determined with the predicted temperature by the 2D heat transfer model and the relationship of "density-temperature" in Figure 3(b). Therefore, the theoretical reduction amount at any position along the slab width direction could be easily determined with Eq.(9).

It should be noted that different values of  $N$  ( $N=28, 35, 47$ ) were used to solve Eq. (12), and the difference of the calculated results with different  $N$  values was very small. Therefore,  $N=28$  (corresponding to element side of 5mm of the heat transfer model in Figure (2)) was adopted for decreasing the total number of the elements of the heat transfer model and the calculation time.

#### 4. Results and Discussion

In the early casting stage, liquid steel in the internal region of the casting strand could flow freely, and the solidification shrinkage in the mushy region could be sufficiently compensated by the free flowing liquid steel from the strand upper stream. However, the flowing liquid steel would be prevented by the developed dendrites-forming network when the solid fraction,  $f_s$ , in the strand center was larger than 0.3 [19, 27], and MSR should be implemented in this casting stage for effectively compensating the volume shrinkage in the mushy region. In the present work,  $f_s$  in the range of 0.3 ~ 1.0 was taken as the reduction zone, and the required theoretical reduction amount and reduction gradient/rate at different positions along the slab width direction, as indicated in Figure 8, were calculated and discussed.

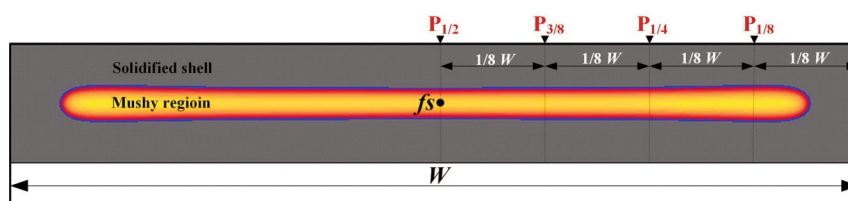


Figure 8. Schematic of the positions where the required theoretical reduction amount were calculated

#### 4.1. Calculated Results

Figure 9 shows the required theoretical reduction amount along the slab width direction at different strand position (corresponding to different solid fraction,  $f_s$ , in the strand center) in the MSR zone, and  $f_s = 0.3$  and  $f_s = 1.0$ , respectively, represent the start and end position of MSR zone.

It can be seen from Figure 9 that the required theoretical reduction amount continuously increased with the increase of  $f_s$  during the implementation of MSR. Additionally, due to the non-uniform solidification of the wide-thick slab, the required theoretical reduction amount in different regions along the slab width direction also differed a lot. In the region of 0 ~ 550 mm from the wide surface center, the variation of the cooling water flux distribution, as indicated in Figure 4(b), was not significant. As a result, the required theoretical reduction amount in this region also changed a little along the slab width direction. With the cooling intensity on the slab surface getting reduced in the region of 550 ~ 700 mm, the volume shrinkage in the strand mushy region in MSR zone also decreased. Therefore, the required theoretical reduction amount showed a downtrend in this region. In the region of 700 ~ 900 mm, the cooling intensity on the wide surface continuously decreased. However, the enhanced cooling effect from the slab narrow surface on the solidification of the residual liquid steel in the mushy region became more and more significant with approaching the slab narrow side. For this reason, more volume shrinkage in the mushy region should be compensated by MSR, which resulted in the fact that the required theoretical reduction amount continuously increased before reaching a maximum value. With further approaching the slab narrow side, the residual liquid steel amount in the mushy region at the beginning of MSR decreased because more liquid steel was solidified before the MSR zone due to the much more enhanced cooling effect from the slab narrow side. As a result, the required theoretical reduction amount for compensating the solidification shrinkage of the residual liquid steel rapidly decreased to zero after it reached a maximum value. In the region of  $\geq 900$  mm, the casting strand was completely solidified at the beginning of MSR, and no volume shrinkage of the residual liquid steel occurred

during the implementation of MSR. Therefore, the required theoretical reduction amount remained zero in this region.

It can be known from the discussion above that the required theoretical reduction amount for the wide-thick slab varied a lot along its width direction due to the non-uniform solidification. This means that the difference of the required theoretical reduction at different positions along the wide-thick slab width direction should be fully considered during the determination of the practical reduction amount for comprehensively improving the internal quality of the wide-thick slab with MSR.

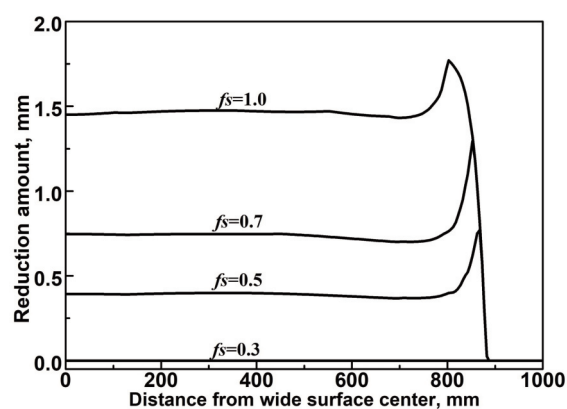


Figure 9. Distribution of the required theoretical reduction amount along slab width direction during the implementation of MSR for 2000mm  $\times$  280mm section size slab under 0.8 m·min<sup>-1</sup>

Reduction gradient and rate [11, 12], respectively, represent the reduction amount per unit strand length and per unit time, which reflected the deformation velocity of the casting strand during the implementation of MSR and provided important theoretical basis for avoiding slab internal cracks and equipment damage caused by the excessive MSR deformation.

Figure 10(a) and (b) show the theoretical reduction gradient and rate at different positions along the slab width direction. During the implementation of MSR, mushy region of the slab transverse section continuously decreased, and the volume shrinkage of the residual liquid steel per unit strand length/time also correspondingly reduced. As a result, the reduction gradient/rate presented a linearly decreasing trend in

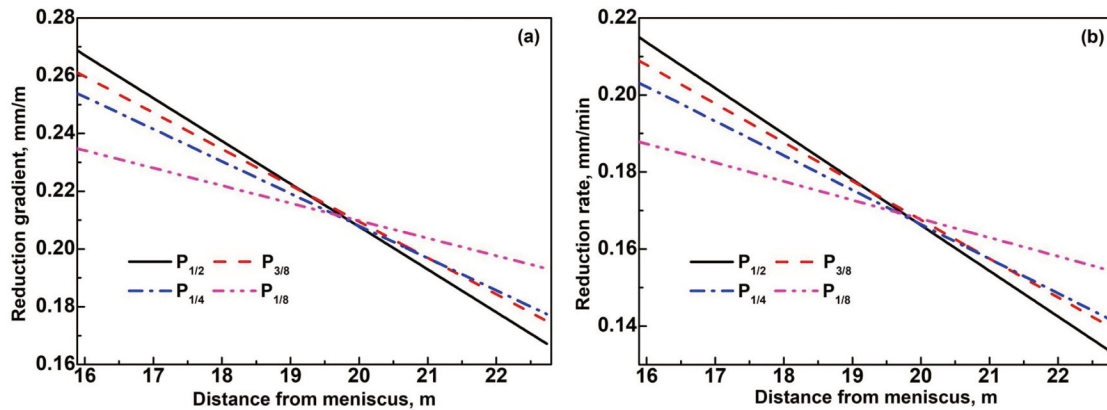


Figure 10. Variation of the theoretical (a) reduction gradient and (b) reduction rate at different positions for 2000mm × 280mm section size slab under 0.8 m·min<sup>-1</sup>

the MSR zone. Furthermore, the cooling intensity continuously decreased from slab surface center to corner, therefore, the order of the theoretical reduction gradient/rate at different positions was  $P_{1/2} > P_{3/8} > P_{1/4} > P_{1/8}$  in the first half of MSR zone. In the second half of MSR zone, although the cooling intensity in the region near the slab surface center was stronger, the thicker solidified shell significantly increased the thermal resistance of the casting strand, and meanwhile more residual liquid steel in the mushy region was already solidified in the first half of MSR zone. For this reason, the required theoretical reduction amount per unit strand length/time for compensating the solidification shrinkage of the residual liquid steel was smaller at the positions near the slab surface center, and the order of the reduction gradient/rate was correspondingly just opposite to that in the first half of the MSR zone.

#### 4.2. Difference between the Previous Methods and the New Method

To illustrate the difference between the previous and the newly-proposed method, theoretical reduction amount and reduction gradient/rate were calculated using Lin's method [11, 12] (as an example of the previous methods) and compared with the calculated results using the newly-proposed method.

Figure 11 compares the calculated theoretical reduction amount using Lin's method with that using the newly-proposed method. Mushy region in the transverse section of the casting strand was usually regarded as a whole in the previous methods. As a result, the calculated theoretical reduction amount using Lin's method was invariable along the slab width direction at each strand position (corresponding to different solid fraction,  $f_s$ , in the strand center) in the MSR zone. This indicated that the previous methods were no longer applicable during the determination of

the theoretical reduction amount for the wide-thick slab because the difference of the required theoretical reduction amount at different positions along the slab width direction could not be taken into consideration.

It also can be seen from Figure 11 that the calculated theoretical reduction amount using Lin's method was usually smaller than that using the newly-proposed method. This was caused by the fact that Lin's method was derived with the assumption that the mass flow of the slab transverse section was invariable during the MSR process, and the mass flow loss caused by the solidification shrinkage in the mushy region could be compensated by the mass flow of all the reduced area of the slab transverse section (the reduced area was calculated by multiplying the slab width by the reduced slab thickness) during the MSR process. However, the width of the mushy region in the slab transverse section was obviously smaller than the slab width, which meant that only the mass flow of the reduced area corresponding to the mushy region could effectively compensate the mass flow loss caused by the solidification shrinkage in the mushy region. As a result, the calculated theoretical reduction amount using Lin's method was smaller than that using the newly-proposed method. Furthermore, the width of the mushy region in the slab transverse section continuously decreased during the MSR process, which enlarged the difference between the slab width and the mushy region length. For this reason, the difference between the calculated theoretical reduction amount using Lin's method and that using the newly-proposed method was also enlarged with the increase of  $f_s$ .

Figures 12(a) and (b) compare the theoretical reduction gradient and rate using the newly-proposed method with that using Lin's method. It can be seen that both the calculated reduction gradient/rate using Lin's method and that using the newly-proposed method

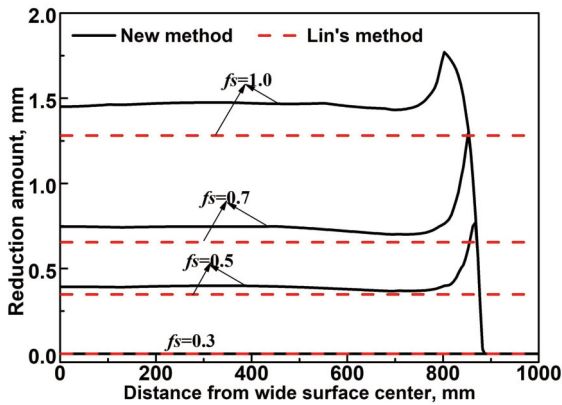


Figure 11. Comparison between the calculated theoretical reduction amount using Lin's method and that using the newly-proposed method for 2000mm × 280mm section size slab under 0.8 m·min<sup>-1</sup>

linearly decreased in the reduction zone. Meanwhile, obvious difference also existed between the calculated results using these two different methods. The calculated reduction gradient/rate at different positions using the newly-proposed method was overall larger than that using Lin's method, and the difference between the calculated results using Lin's method and that at P<sub>1/4</sub> and P<sub>1/8</sub> using the newly-proposed method continuously increased in the MSR zone. This indicated that the centerline segregation and porosity of the wide-thick slab, especially in the region between P<sub>1/4</sub> and P<sub>1/8</sub>, could not be effectively improved if the reduction gradient/rate was determined using Lin's method during the implementation of MSR.

### 4.3. Effect of Casting Speed

To investigate the effect of casting speed, theoretical reduction amount/gradient/rate at P<sub>1/2</sub> of the 2100 mm × 280 mm section size slab under

different casting speeds were calculated and compared using the newly-proposed method.

Figure 13(a) shows the theoretical reduction amounts under different casting speeds. It can be seen that, with the casting speed increased, both the start position and end position of MSR zone moved afterwards along the casting direction, and the length of MSR zone, which is shown in Figure 13(b) and represents the strand length between the start position and the end position of MSR zone, increased significantly by 10% from 6.0 m to 7.7 m when the casting speed was increased from 0.7 m·min<sup>-1</sup> to 0.9 m·min<sup>-1</sup>. Compared with the length of MSR zone, the variation of mushy region thickness at the start position of MSR zone with casting speed was not significant and remained around 74.3 mm. As a result, the total required theoretical reduction amount at the end of MSR zone, as shown in Figure 13(a), for compensating the volume shrinkage in the mushy region also changed a little and remained around 1.5 mm under different casting speeds.

Figures 14(a) and (b) show the reduction gradient and reduction rate under different casting speeds. It can be seen that both the reduction gradient and reduction rate under different casting speeds linearly decreased in the MSR zone. However, with the casting speed increased, the decrease of theoretical reduction gradient in Figure 14(a) became slower.

To conveniently and quantitatively compare the influence of casting speed, the average reduction gradient and rate under different casting speeds, as shown in Figure 14(c), were calculated based on the theoretical reduction gradient/rate in Figure 14(a) and (b). The required total theoretical reduction amount under different casting speeds, as shown in Figure 13(a), were almost the same, but the length of MSR zone, as shown in Figure 13(b), significantly increased when the casting speed increased. As a result, the average theoretical reduction gradient,

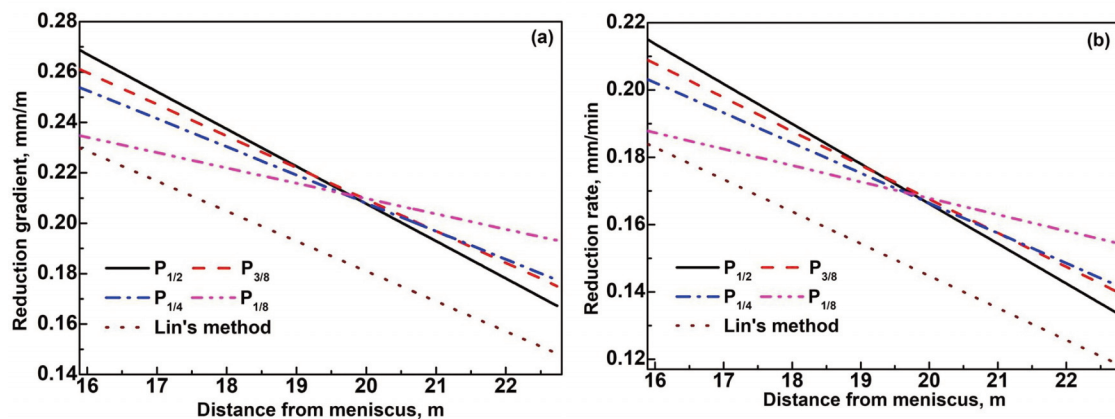


Figure 12. Comparison of the calculated (a) reduction gradient and (b) reduction rate using Lin's method and the newly-proposed method for 2000mm × 280mm section size slab under 0.8 m·min<sup>-1</sup>



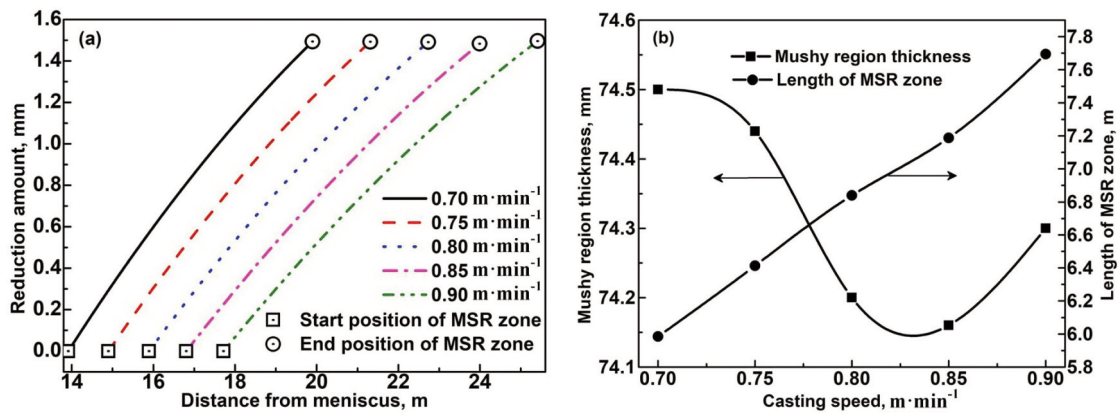


Figure 13. Variation of (a) theoretical reduction amount, (b) the mushy region thickness at the start position of MSR zone and length of MSR zone under different casting speeds

which represented the required theoretical reduction amount per unit strand length in MSR zone, almost decreased linearly from 0.25 mm/m to 0.19 mm/m when the casting speed increased from 0.70 m·min<sup>-1</sup> to 0.90 m·min<sup>-1</sup>. When the casting speed increased, the cooling water flux (that denoted the cooling water amount per unit time in unit strand surface area) in secondary cooling zones also slightly increased for

enhancing the cooling intensity of the strand surface, but the variation of cooling water flux was not so significant as that of the length of MSR zone. This means that the required compensated volume shrinkage in the mushy region per unit time also varied a little. As a result, the variation of the average theoretical reduction rate with casting speed, as shown in Figure 14(c), was not significant.

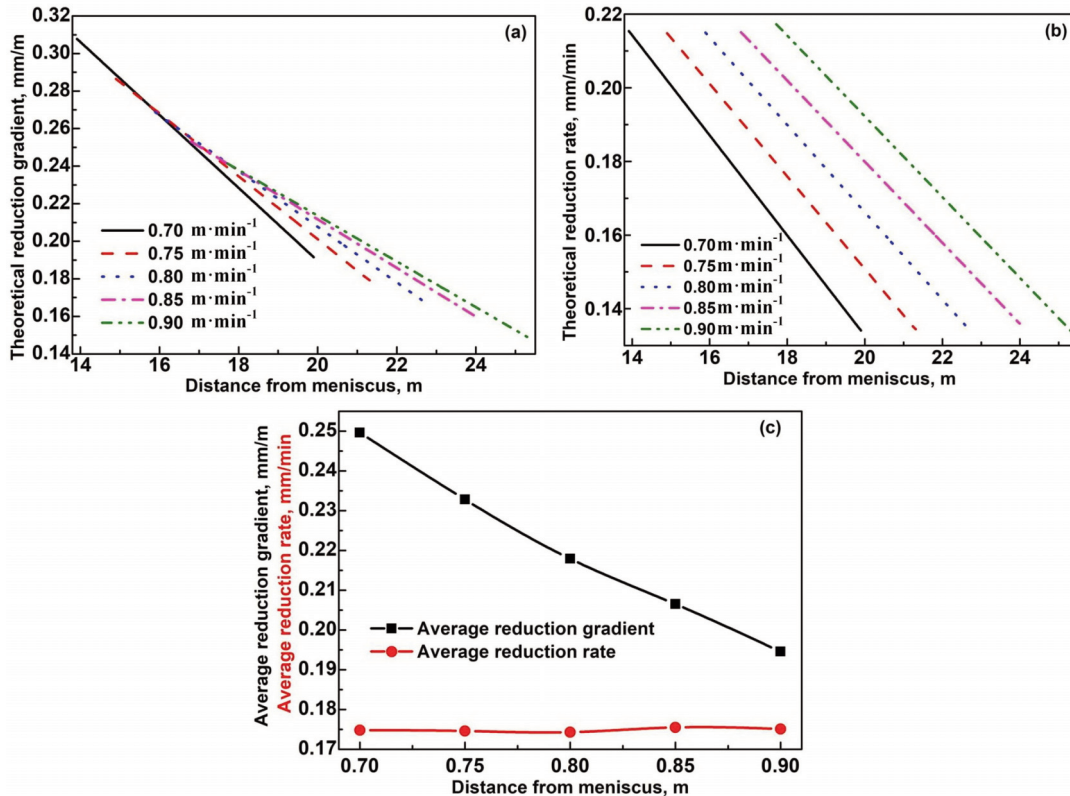


Figure 14. Variation of (a) theoretical reduction gradient, (b) theoretical reduction rate and (c) average theoretical reduction gradient/rate under different casting speeds



## 5. Conclusions

In the present work, a 2D heat transfer model was developed for predicting the non-uniform solidification of the wide-thick slab, and then a new method for determination of the theoretical reduction amount of the wide-thick slab under non-uniform cooling conditions was presented. Based on the predicted temperature field by the 2D heat transfer model and the newly-proposed calculation method of theoretical reduction amount, the required theoretical reduction amount and reduction gradient/rate for the wide-thick slab were calculated and discussed. Some main conclusions are summarized as follows:

1) Due to the non-uniform solidification of the wide-thick slab, the required theoretical reduction amount in different regions along the slab width direction also differed a lot. The theoretical reduction amount changed a little in the region of 0 ~ 550 mm from slab surface center, presented a downtrend in the region of 550 ~ 700 mm and firstly continuously increased to reach a maximum value and then rapidly decreased to zero in the region of 700 ~ 900 mm;

2) The theoretical reduction gradient/rate at different positions of the wide-thick slab linearly decrease in the MSR zone, and the order of them was  $P_{1/2} > P_{3/8} > P_{1/4} > P_{1/8}$  in the first half of MSR zone and  $P_{1/2} < P_{3/8} < P_{1/4} < P_{1/8}$  in the second half of MSR zone;

3) The calculated theoretical reduction amount and reduction gradient/rate with Lin's method were overall smaller than that with the newly-proposed method, and the difference between the theoretical reduction gradient/rate with Lin's method and that at  $P_{1/4}$  and  $P_{1/8}$  with the newly-proposed method continuously increased in the MSR zone;

4) When the casting speed increased from 0.70  $\text{m}\cdot\text{min}^{-1}$  to 0.90  $\text{m}\cdot\text{min}^{-1}$ , the total theoretical reduction amount and the average theoretical reduction rate changed a little, but the average theoretical reduction gradient decreased significantly from 0.25 mm/m to 0.19 mm/m.

## References

- [1] W. Bleck, W. Wang, R. Bülte, Steel Res. Int., 77(7) (2006) 485-491.
- [2] R. Thome, K. Harste, ISIJ Int., 46(12) B (2006) 1839-1844.
- [3] R. Thome, K. Harste, Steel Res. Int., 75(10) (2004) 693-700.
- [4] V. Ludlow, A. Normanton, A. Anderson, M. Thiele, J. Ciriza, J. Larraudogoitia, W. Knoop, Ironmaking Steelmaking, 32(1) (2005) 68-74.
- [5] S. Luo, M. Zhu, C. Ji, Ironmaking Steelmaking, 41(3) (2014) 233-240.
- [6] M. C. Flemings, ISIJ Int., 40(9) (2000) 833-841.
- [7] T. Han, C. Cheng, J. Mei, J. Zhu, Y. Jin, Adv. Mater. Res., 881 (2014) 1558-1561.
- [8] C. Ji, S. Luo, M. Zhu, Y. Sahai, ISIJ Int., 54(1) (2014) 103-111.
- [9] R. Nyström, K. Spitzer, Steel Res. Int., 74(11-12) (2003) 700-707.
- [10] Z. Xu, X. Wang, M. Jiang, Steel Res. Int., 88(2) (2017) 231-242.
- [11] Q. Lin, M. Zhu, Acta Metall. Sin., 43(8) (2007) 847-850.
- [12] Q. Lin, M. Zhu, Acta Metall. Sin., 43(12) (2007) 1297-1300.
- [13] Y. Ito, A. Yamanaka, T. Watanabe, Rev. Metall., 97(10) (2000) 1171-1176.
- [14] Q. Lin, M. Zhu, Acta Metall. Sin., 43(12) (2007) 1301-1304.
- [15] Q. Lin, M. Zhu, Iron Steel, 2010(3) B (2010) 32-37.
- [16] B. Wang, J. Zhang, Y. Yin, Q. Dong, C. Xiao, Metall. Res. Technol., 113(4) (2016) 406.
- [17] K. Liu, J. Zhang, Adv. Mater. Res., 482 (2012) 859-862.
- [18] C. Ji, S. Luo, M. Zhu, ISIJ Int., 54(3) (2014) 504-510.
- [19] K. Liu, Q. Sun, J. Zhang, C. Wang, Metall. Res. Technol., 113(5) (2016) 504.
- [20] K. Liu, Q. Sun, L. Wang, J. Zhang, J. Iron Steel Res., 92(2) (2017) 111-116.
- [21] C. Ji, M. Zhu, TMS Annual Meeting and Exhibition 2010, 14-18 Feb., Seattle, USA, 2010, p. 275-282.
- [22] B. Rogberg, L. Ek, ISIJ Int., 58(3) (2018) 478-487.
- [23] C. Wu, C. Ji, M. Zhu, Steel Res. Int., 88(9) (2017) 1600514.
- [24] H. Wang, G. Li, Y. Lei, Y. Zhao, Q. Dai, J. Wang, ISIJ Int., 45(9) (2005) 1291-1296.
- [25] C. Li, B. G. Thomas, Metall. Mater. Trans. B, 35(6) (2004) 1151-1172.
- [26] S. Louhenkilpi, J. Miettinen, L. Holappa, Trans. Iron Steel Inst. Jpn., 46(6) (2006) 914-920.
- [27] Z. Han, D. Chen, K. Feng, M. Long, ISIJ Int., 50(11) (2010) 1637-1643.



## NOVI METOD ZA UTVRĐIVANJE TEORIJSKOG PROCENTA REDUKCIJE ZA VELIKI SLAB TOKOM POSTUPKA MEHANIČKE REDUKCIJE

C.-H. Wu \*, J.-H. Zeng, G.-R. Wu, X. Xie, M. Zhang

Istraživački institut kompanije Pangang Group, Ltd., Pandžihua, Sečuan, Kina

### Apstrakt

Mehanička meka redukcija (MSR) predstavlja efikasnu metodu za uklanjanje centralne segregacije i poroznosti kod kontinuirano livenog čeličnog slaba, a procenat redukcije predstavlja ključni parametar koji određuje uspešnost primene ove tehnike. U ovom radu je razvijen 2D model prenosa toplote za predviđanje nejednakog očvršćavanja velikog slaba. Debljina ljuske je izmerena metodom zakivanja, dok je temperatura na površini slaba izmerena infracrvenom kamerom, nakon čega su ovi podaci upotrebljeni za validaciju 2D modela za prenos toplote. Nakon toga je izvedena nova metoda za proračun teorijskog procenta redukcije koja bi u obzir uzela nejednako očvršćavanje kod velikog slaba. Na osnovu predviđenog temperaturnog polja dobijenog pomoću 2D modela za prenos toplote i novog modela za proračun, izračunati su i uzeti u obzir neophodan teorijski procenat redukcije, kao i stepen/brzina redukcije za veliki slab. Takođe je ispitana razlika između nove metode i metode koja je prethodno korišćena, kao i uticaj brzine livenja i debljine slaba na neophodan teorijski procenat redukcije i stepen/brzinu redukcije.

**Ključne reči:** Teorijski procenat redukcije; Mehanička meka redukcija; Kontinuirano livenje; Veliki slab; Nejednako očvršćavanje

